

Vortex dynamics associated with the collision of a sphere with a wall

Thomas Leweke

Institut de Recherche sur les Phénomènes Hors Equilibre, UMR 6594 CNRS/Universités Aix-Marseille, 49 rue F. Joliot-Curie, B.P. 146, F-13384 Marseille Cedex 13, France

Mark C. Thompson and Kerry Hourigan

Fluids Laboratory for Aeronautical and Industrial Research (FLAIR), Department of Mechanical Engineering, Monash University, Melbourne, 3800, Australia

(Received 11 May 2004; accepted 26 May 2004; published online 6 August 2004)

For moderate Reynolds numbers, a sphere striking a wall in the normal direction leads to the trailing recirculating wake threading over the sphere and developing into a complex vortex ring system as it interacts with the wall. The primary vortex ring, which consists of vorticity from the wake, persists and convects slowly outwards away from the sphere due to the motion induced from its image. The structure and evolution of this vortex system is quantified through a combined experimental and numerical study. At higher Reynolds numbers a non-axisymmetric instability develops, which leads to rapid dispersion of the ring system. A comparison of the wavelength and growth rate, predicted from both linear stability theory and direct simulations, with idealized models indicates that the mechanism is dominated by a centrifugal instability at the edge of the primary vortex core. © 2004 American Institute of Physics. [DOI: 10.1063/1.1773854]

When a rigid body collides with a surface, a layer of dust on the surface can be resuspended due to the effects of two different mechanisms. The first is ballistic, where the collision breaks cohesive bonds between the dust particles. If the kinetic energy is sufficiently large, this can lead to the ejection of particles from the wall. The second mechanism is hydrodynamic; this is the focus of the current study. At Reynolds numbers (based on impact speed and sphere diameter) in excess of approximately 100, the wake flow following the rigid body overtakes it on impact and resultant ring vortex structure(s) can cause significant fluid exchange near the surface leading to dust resuspension. Eames and Dalziel¹ have examined the behavior in detail as the Reynolds number was varied between 300 and 3500. Their analysis was mainly directed toward resuspension characteristics of different dust types and layer thicknesses, rather than the fluid dynamics, which is of primary concern for this Letter. Other recent experimental studies^{2,3} were concerned with the rebound characteristics of a particle in a fluid, and it was found that the coefficient of restitution of such collisions was a function of the Stokes number. The vortex ring system generated during the impact shows similarities to that produced from the impact of a vortex ring with a wall, examined in a number of previous studies.⁴⁻⁷ The similarities and differences will be discussed. Note that particle impacts with walls also have potential importance for other areas of fluid mechanics such as enhancement of heat transfer due to the convection of fluid toward and away from a surface.

This Letter focuses mainly on two aspects of the particle-wall interaction: (a) the formation and evolution of the vortex system associated with the impact, and (b) the characterization and interpretation of a three-dimensional instability, which leads to the rapid diffusion of the main vortex rings for $Re \geq 1000$.

The experiments were carried out in a water tank with

glass walls of dimensions $500 \times 500 \times 600 \text{ mm}^3$. A bronze ball 19.02 mm in diameter (D) was attached to an inelastic plastic string, which passed over a pulley and was wound on a threaded reel driven by a high-resolution computer-controlled stepper motor. This mechanism allowed the sphere to be lowered through the water at a specified uniform speed (U), thereby allowing selection of the Reynolds number. Fluorescein dye coupled with light from an argon ion laser was used to visualize the wake, and the formation and advection of the vortex ring structures.

Existing spectral-element software⁸⁻¹⁰ was modified to perform the direct numerical simulations (DNS). The movement of the sphere relative to the wall was treated using the Arbitrary Lagrangian Eulerian approach.¹¹ As the sphere approaches the surface, the vertices of the mesh move with predetermined specified velocities so that the semi-circular boundary of the sphere (in the axisymmetric coordinate system) is maintained and the distortion of the mesh is controlled. It was necessary to remesh several times as the sphere approached the wall, to avoid excessive skewness of the spectral elements. The computational boundaries were placed sufficiently far from the sphere so that the blockage was considerably less than 1%. The sphere was stopped at a distance of $0.005D$ from the wall to avoid the development of a mesh singularity over the final few timesteps. Both experimental and computational tests were conducted to verify that this had negligible influence on the predictions.

The important parameters controlling the interaction are the impact distance L/D , where L is the initial distance between the bottom of the sphere and the wall, and the Reynolds number, $Re = UD/\nu$, where ν is the kinematic viscosity. The initial focus is on the case with $Re = 800$, $L/D = 5$. For this parameter set, the flow remains axisymmetric throughout the evolution, yet the Reynolds number is sufficiently large to allow a complex vortex ring system to develop.

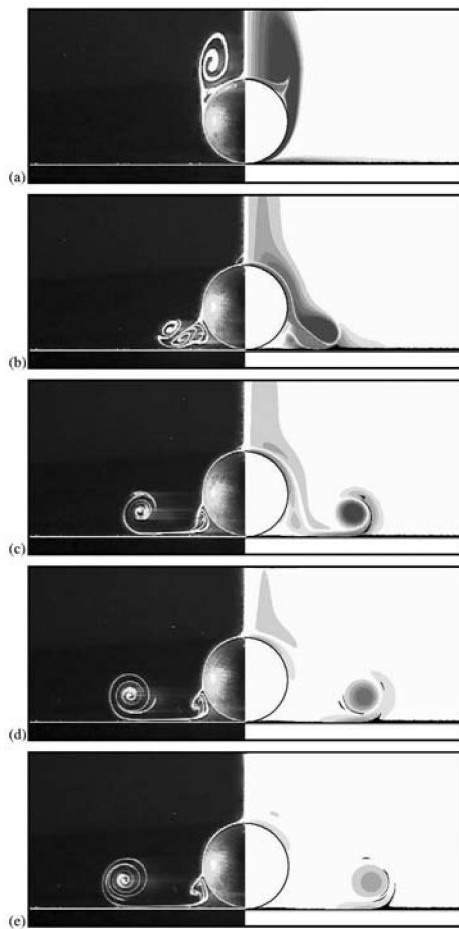


FIG. 1. Evolution of the flow after impact of the sphere for $Re=800$, $L/D=5$. Left: experimental dye visualization; right: azimuthal vorticity from DNS and tracer particles initially in a layer near the wall. (a) $\tau=0$, (b) $\tau=2$, (c) $\tau=5$, (d) $\tau=10$, (e) $\tau=16$.

Figure 1 shows the evolution of the flow for this benchmark case. The left-hand images contain visualizations obtained by coating the surface of the sphere with a mixture containing fluorescein dye and using a laser light sheet to highlight the flow structures. The right-hand images were obtained from DNS simulations; they show instantaneous vorticity fields together with positions of tracer particles placed initially in a layer near the wall. Here, $\tau=tU/D$ is the non-dimensional time. Note that numerical simulations (not shown) with particles initially placed on the sphere surface are virtually identical to the dye visualizations; this provides further confidence in the numerical predictions. The simulations clearly show the presence of considerable secondary vorticity induced when the primary vortex ring originating from the attached recirculation bubble of the sphere approaches the wall. At $\tau=5$, Fig. 1(c) shows this secondary vorticity partially encasing the primary vortex core. The secondary vorticity is not apparent from the dye visualizations, however, the kink in the outmost dye line in the left-hand image and the isolated blob of tracer particles in the right-hand image are associated with its presence. At later times the secondary vorticity continues to be drawn up to encircle the primary vortex ring, but the effect of diffusion and cross-annihilation rapidly reduce the strength of both the primary

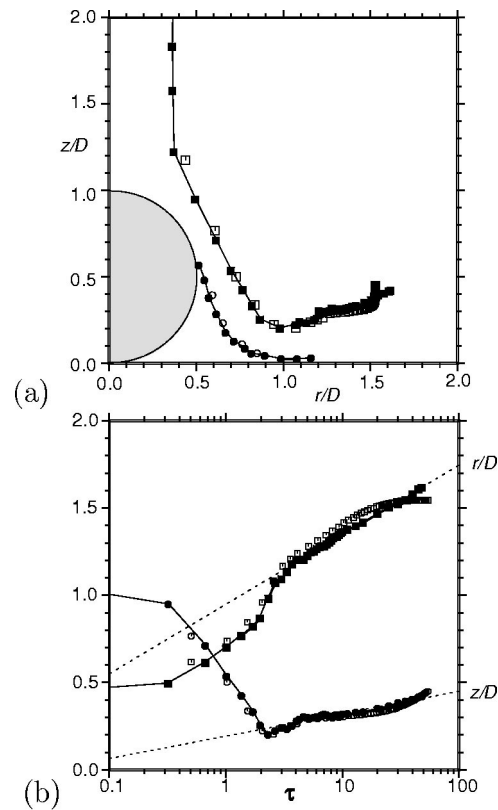


FIG. 2. (a) Trajectories of vortex centers for $Re=800$, $L/D=5$, and up to $\tau=50$. Primary wake vortex (\blacksquare : exp., \square : DNS) and secondary vortex from sphere surface (\bullet : exp., \circ : DNS). (b) Radial (r) and vertical (z) position of primary wake vortex as function of time, from experiment (closed symbols) and DNS (open symbols). Dashed lines are logarithmic fits to the experimental data for $\tau>3$.

and secondary vortical structures. For this Reynolds number/starting distance combination, the secondary vorticity does not fragment as it does for the related case of an isolated vortex ring impinging on a wall.⁴⁻⁷ This fragmentation is observed at higher Reynolds numbers and/or significantly greater starting distances. The separation of the flow at the wall outside the primary ring is clearly shown in both the dye and passive tracer visualizations; this is the cause of the dust resuspension studied in Ref. 1.

Figure 2(a) shows the trajectories of the vortex centers for the same $Re-L/D$ combination. The primary ring effectively bounces off the wall as it propagates radially outwards from the sphere. Again, this shows some similarity to the bounce observed when an isolated vortex ring strikes a wall.⁴⁻⁷ However, in that case the bounce appears to be transitory. The mechanism is likely to be the same, i.e., the velocity induced at the primary ring center by the secondary vorticity as it is drawn up from the boundary. Figure 2(b) shows the long term evolution of the axial (z/D) and radial (r/D) positions for the primary vortex ring. Broadly, there are two regimes: before the primary ring impact, at approximately $\tau=2$, and after ring impact. The experimental dye visualizations indicate that the primary ring will continue to advect both axially and radially away from the sphere even at long times. However, experimentally it is difficult to obtain accurate data for long times because the velocities in-

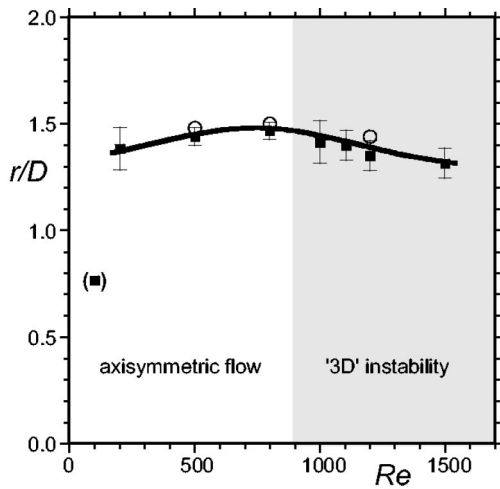


FIG. 3. Radius of the primary wake vortex at $\tau=20$ as function of Re , for $L/D=5$. Experiment (■) and axisymmetric DNS (○).

duced by the vortex system become comparable to noise introduced by factors such as convection currents caused by small temperature non-uniformities. In contrast, numerical predictions of the position of maximum vorticity in the core indicate that radial expansion of the primary ring almost ceases after $\tau=15$. By this time the vorticity field has decayed substantially due to diffusion and cross-annihilation with secondary vorticity generated at the boundary, and the total circulation of the image vortex, which is the primary cause for the outward convection of the ring vortex, has dropped to very low values. Figure 2(a) shows that the trajectory becomes almost vertical for large times. This is presumably due to the preferential cross-annihilation of vorticity that takes place near the boundary which has the consequence of pushing the centroid of the remaining primary vorticity further from the boundary. This effect is unlikely to be captured experimentally by using dye to monitor the position of the primary ring, which may explain the slight difference between numerical and experimental results.

Figure 3 shows the radius of the primary vortex ring after a relatively long time of $\tau=20$, as a function of Reynolds number. The radial convection velocity is not very sensitive to this parameter; over the range investigated ($200 < Re < 1500$) the primary ring radial position was $(1.4 \pm 0.1)D$ at $\tau=20$. Both the numerical and experimental results indicate the primary vorticity ring propagates furthest away from the impact position for $Re \approx 800$. In the experiments, however, the flow did not remain axisymmetric at all times for $Re > 900$.

The three-dimensional structure that develops at higher Reynolds numbers is depicted in Fig. 4 (see Ref. 12 in this issue). In (a), a dye visualization is shown for $Re=1500$, $L/D=5$, and $\tau=9$, and (b) shows radial vorticity isosurfaces obtained from numerical simulations for the same L/D and τ , and at $Re=1200$, the highest Reynolds number simulated. For the latter, the velocity field is initially seeded with a low-level white noise perturbation to initiate the development of the instability. The dye pattern indicates that the maximum growth occurs outside the primary vortex core, and is presumably associated with the secondary vorticity

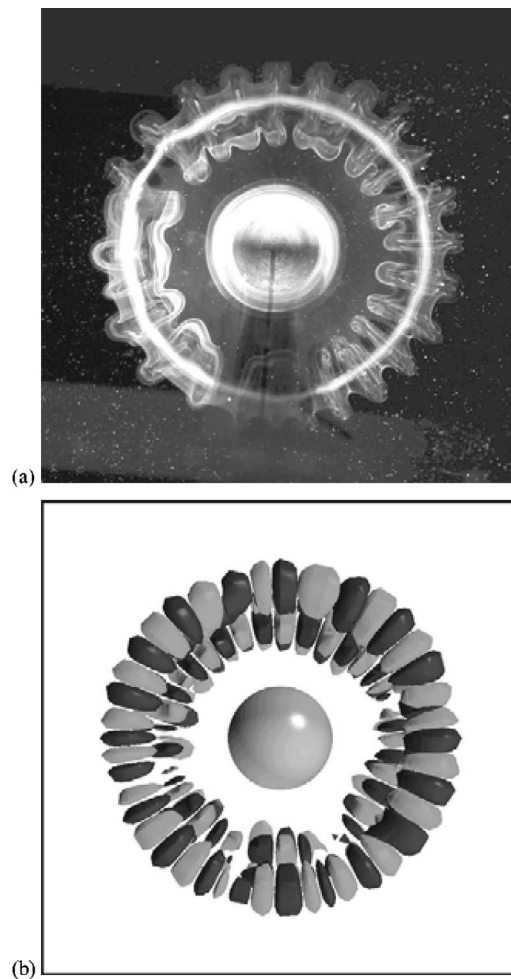


FIG. 4. Instability of the axisymmetric flow for sphere impact without rebound and $L/D=5$. (a) Experimental dye visualization at $\tau=9$ for $Re=1500$; (b) perturbation radial vorticity from DNS at $\tau=9$ for $Re=1200$.

drawn up from the boundary. The wavelength is approximately $0.4D$, but varies considerably at different azimuthal positions. This is much smaller than the typical instability wavelength associated with vortex-ring wall interactions,⁷ which has been attributed to rapid distortion of a secondary vortex ring by the strain induced by the strong and more stable primary vortex.

To investigate this further, a linear stability analysis was performed on a series of “frozen” axisymmetric base flows at different times after impact. The time-averaged amplitude multiplication factor per unit time was determined as a function of azimuthal wavenumber m . The predictions are shown in Fig. 5 for a series of discrete times. The maximum amplification occurs at $\tau=4$ for $m \approx 20$. The growth rate curves are broadband, consistent with the observed experimental and DNS variations in the selected wavelength. In addition, the dominant wavenumber gives wavelengths consistent with both the DNS simulations and the dye visualizations.

The perturbation azimuthal vorticity field of the (pseudo-)eigenmode is shown in Fig. 6, for $\tau=4$ and $m=20$. This perturbation amplitude is clearly strong within the primary vortex core and strongest at the edge of the core, where the vorticity changes sign. For this wavelength, the mode is

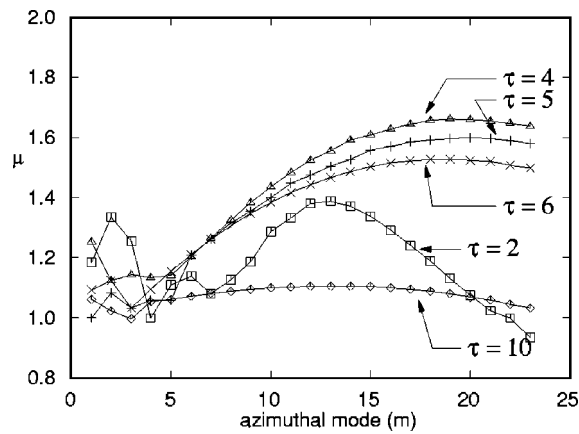


FIG. 5. Amplification factor per unit time (μ) associated with the frozen axisymmetric base flow as function of azimuthal mode number and non-dimensional time. Here, $Re=1200$ and $L/D=5$.

not stationary but revolves with the core. Maximum instantaneous growth occurs when the perturbation within the core is aligned with the principal strain induced by the external vorticity field, and especially by the image vortex ring underneath the surface. This situation corresponds approximately to the image shown in the figure; the principal stretching axis of the strain and the line joining the inner extrema of the vorticity perturbation are aligned at about 45° to the horizontal. Also shown is a contour of approximately zero perturbation, an “invariant” stream tube, depicted as an overlaid ellipse.

This pattern is consistent with the predicted perturbation field for an elliptic instability of a strained vortex.¹³ Interestingly, according to the theory of elliptic instability (neglecting the curvature of the vortex ring), the preferred wavelength should correspond to approximately twice the diameter of the invariant stream tube. This gives $m \approx 20$, consistent with the observed wavelength for this mode. However, both analytical theory¹⁴ and numerical stability analysis of the velocity field associated with the vorticity of the primary vortex core only, show that the predicted growth rate of elliptic instability for the present case is clearly negative.

Alternatively, we have performed a stability analysis of an *axisymmetric* flow field, associated with the mean vorticity, i.e., the average in the circumferential direction around the location of the primary vortex center in the $r-z$ plane (see Fig. 1), including both positive and negative contributions. Such an analysis effectively investigates the stability of the flow to a centrifugal instability. For the flow at $Re=800$, $L/D=5$, and $\tau=4$, i.e., for a structure close to the one in Fig. 1(c), a strongly positive growth rate, in excess of the levels shown in Fig. 5, is obtained, with a preferred wavelength within $0.1D$ of the predicted wavelength of the actual base flow field. Thus, although the instability is clearly complex, in terms of basic physical mechanisms, it appears that it can be interpreted as driven by a centrifugal instability of the vorticity field in the neighborhood of the primary core, but with substantial modification associated with a subsequent elliptic instability of the core. More quantitative evidence for this viewpoint will be provided in a followup paper.

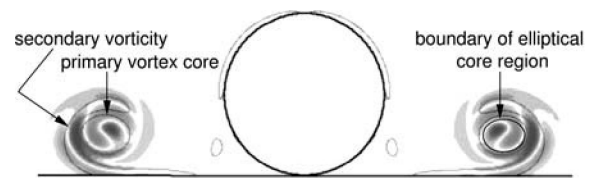


FIG. 6. Structure of the perturbation azimuthal vorticity field corresponding to the dominant eigenmode for $Re=1200$, $L/D=5$, $m=20$, and $\tau=4$. Contours of positive and negative azimuthal vorticity for the base flow are shown to indicate the positions of the primary vortex ring and encircling secondary vorticity. The overlaid elliptical contour on the right shows the *invariant stream tube*.

In summary, we have made detailed observations of the flow generated by the collision of a sphere with a solid surface at low Reynolds numbers and running distances, showing the interaction of the primary axisymmetric wake vortex with secondary vorticity generated on the sphere and the surface after impact. The wake vortex ring is found to expand to a maximum diameter of about three sphere diameters, with only a weak Reynolds number dependence. For Re around 1000 and above, a three-dimensional instability of azimuthal wave number $m \approx 20$ is observed. Stability investigations suggest that the origin is a centrifugal instability of the primary vortex ring, due to the presence of the opposite-signed secondary vorticity.

This work was supported by grants from the Australian Research Council (Grant No. LX0242362) and the French CNRS (Grant No. DRI 11721). The authors thank the Victorian and Australian Partnerships for Advanced Computing (VPAC and APAC) for supplying computing resources for this project.

- ¹I. Eames and S. B. Dalziel, “Dust resuspension by the flow around an impacting sphere,” *J. Fluid Mech.* **403**, 305 (2000).
- ²G. G. Joseph, R. Zenit, M. L. Hunt, and A. M. Rosenwinkel, “Particle-wall collisions in a viscous fluid,” *J. Fluid Mech.* **433**, 329 (2001).
- ³P. Gondret, M. Lance, and L. Petit, “Bouncing motion of spherical particles in fluids,” *Phys. Fluids* **14**, 643 (2002).
- ⁴J. D. Walker, C. R. Smith, A. W. Cerra, and T. L. Dogilaski, “The impact of a vortex ring on a wall,” *J. Fluid Mech.* **181**, 99 (1987).
- ⁵T. T. Lim, T. B. Nichols, and M. S. Chong, “A note on the cause of the rebound in the head-on collision of a vortex ring with a wall,” *Exp. Fluids* **12**, 41 (1992).
- ⁶P. Orlandi and R. Verzicco, “Vortex rings impinging on walls: Axisymmetric and three-dimensional simulations,” *J. Fluid Mech.* **256**, 615 (1993).
- ⁷J. D. Swearingen, J. D. Crouch, and R. A. Handler, “Dynamics and stability of a vortex ring impacting a solid boundary,” *J. Fluid Mech.* **297**, 1 (2000).
- ⁸G. J. Sheard, M. C. Thompson, and K. Hourigan, “From spheres to circular cylinders: Classification of bluff ring transitions and structure of bluff ring wakes,” *J. Fluid Mech.* **492**, 147 (2003).
- ⁹M. C. Thompson, T. Leweke, and M. Provansal, “Kinematics and dynamics of sphere wake transition,” *J. Fluids Struct.* **15**, 575 (2001).
- ¹⁰M. C. Thompson, T. Leweke, and C. H. K. Williamson, “The physical mechanism of transition in bluff body wakes,” *J. Fluids Struct.* **15**, 607 (1999).
- ¹¹T. C. Warburton and G. E. Karniadakis, “Spectral simulations of flow past a cylinder close to a free surface,” *ASME Paper FEDSM97-3389* (1997).
- ¹²T. Leweke, M. C. Thompson, and K. Hourigan, “Touchdown of a sphere,” *Phys. Fluids* **16**, S5 (2004).
- ¹³R. R. Kerswell, “Elliptical instability,” *Annu. Rev. Fluid Mech.* **34**, 83 (2002).
- ¹⁴S. Le Dizès, “Non-axisymmetric vortices in two-dimensional flows,” *J. Fluid Mech.* **406**, 175 (2000).